Morphology is a Link to the Past: examining formative and secular galactic evolution through morphology

A THESIS
SUBMITTED TO THE FACULTY OF THE GRADUATE SCHOOL
OF THE UNIVERSITY OF MINNESOTA
BY

Melanie A. Galloway

IN PARTIAL FULFILLMENT OF THE REQUIREMENTS
FOR THE DEGREE OF
Doctor of Philosophy

Advisor:
Lucy Fortson

month, 2017

Acknowledgements

Some acknowledgements

Dedication

Firstly dedicated to Zuko, for being the sweetest little bird.

Abstract

Galaxy morphology is one of the primary keys to understanding a galaxy's evolutionary history. External mechanisms (environment/clustering, mergers) have a strong impact on formative evolution of the major galactic components (disk, bulge, Hubble type), while internal instabilities created by bars, spiral arms, or other substructures drive secular evolution via the rearrangement of material within the disk. This thesis will explore several ways in which morphology may impact the dynamics and evolution of a galaxy using visual classifications from several Galaxy Zoo projects. Section 1 will focus on the present morphology of galaxies in the local Universe ($z < 0.2$) using data from Galaxy Zoo 2 and Galaxy Zoo UKIDSS. Section 2 will examine populations of morphologies at various lookback times, from $z = 0$ out to $z = 1$ using data from Galaxy Zoo Hubble.

We first explore the impact of bars in disc galaxies on channeling gas from the outer regions of the disk to the inner few kpc necessary to fuel an active galactice nucleus (AGN). Using a sample of 19,756 disk galaxies at $0.01 < z < 0.05$ imaged by the Sloan Digital Sky Survey and morphologically classified by Galaxy Zoo 2, the difference in AGN fraction in barred and unbarred disks was measured. A weak, but statistically significant, effect was found in that the population of AGN hosts exhibited a 16.0% increase in bar fraction as compared to their unbarred counterparts at fixed mass and color. These results are consistent with a cosmological model in which bar-driving fueling contributes to the fueling of growing black holes, but other dynamical mechanisms must also play a significant role.

We study the wavelength dependence on morphology by comparing the optical morphological classifications from GZ2 to classifications done on infrared images in GZ:UKIDSS. We find some cool result. [to be continued]

We examine more directly the morphological changes in galaxy populations as a function of their age using classifications from Galaxy Zoo: Hubble. A sample of XX,XXX disc galaxies from the COSMOS field at $0 < z < 1$ were identified as active or passive using a NUV-r / r -J diagnostic with rest-frame colors from the UltraVISTA catalog. We find that the fraction of disks that are passive increases/decreases from X.X% at

$z = 1$ to X.X% at $z = 0$. We intepret this result as [something having to do with the transformation of disk to elliptical, depending on result]. Addionally, we emphasize the challenges of visual classification that are particular to galaxies at high redshift. We present a correction technique to address these biases using simulated images of nearby SDSS galaxies which were artificially redshifted using the FERENGI code and classified in GZH.

Contents

List of Tables

List of Figures

Chapter 1

Introduction

The Intro

Chapter 2

Bar AGN project

Basically Galloway et al. 2015 Muzahid et al. (2015)

Chapter 3

UKIDSS

UKIDSS science and debiasing.

Chapter 4

Using FERENGI to correct f_{features} for redshift-induced classification bias

4.0.1 Intro

The GZ vote fraction f_{features} plays a crucial role in the majority of science cases that use Galaxy Zoo classifications. It represents the fraction of users who answered "feature or disk" to the first question in the decision tree, and is used to distinguish elliptical/spheroidal galaxies from those with features. Many studies aim to measure the popluation of galaxies exhibiting certain features such as bars (examples), spiral arms (examples), [dump stuff in this list]. In each of these, f_{features} is necessary for creating the sample of galaxies which could potentially contain the feature in question. This is typically acheived by setting a cut, such that all galaxies with f_{features} greater than that threshold are considered to be candidates for that study.

While f_{features} is not a true probability, the measurement is intended to be consistent among all galaxies; that is, two galaxies with similar f_{features} values should have similar likelihoods of being featured (or not featured). This has been shown to be true at low redshift by comparing the f_{features}values to expert classifications (reference Willet et al. 2013); there is a strong correlation between this vote fraction and whether the galaxy was expertly classified as a disk or an elliptical [expand on what W13 actually did.].

For distant galaxies, however, we observe that $f_{\rm features}$ is not consistant with nearby galaxies. As galaxies are observed at higher redshift, the images are inherently less resolved, and smaller features are more difficult to identify. This causes in a decrease in $f_{\rm features}$ than what would be expected if the galaxy had been observed at $z = 0$. Figure [make a figure] shows this effect: [describe some figure, probably a bunch of galaxies that are obviously spirals but with very diff. ffeatures values at diff. redshifts.] Therefore, two identical galaxies, imaged at different redshift, may have small to drastic differences in their $f_{\rm features}$ measurement. In order to keep $f_{\rm features}$ a value correlated with the likelihood of having features that is consistent for *all* galaxies, this bias must be corrected.

A method for correcting redshift bias in the GZ vote fractions was developed and implemented in prior Galaxy Zoo projects (cite GZ1 and GZ2), which contained nearby ($z < 0.2$) galaxies imaged by the SDSS. A correction factor to the classification fractions measured at the higher redshifts was applied by matching the mean vote fractions of those at the lowest redshift. This technique was valid under the assumption that, within this redhisft range, there would be no cosmological evolution of galaxies, and therefore any change in the mean vote fraction for any morphology with redshift was purely due to this observational bias, and not due to a genuine difference in morphological populations.

In GZH, the redshift range is large enough that cosmological evolution of the morphologies of galaxies is expected, and therefore the previous method of correcting redshift-bias will not work. Instead, we have developed a new method of measuring the change in $f_{\rm features}$ as a function of redshift using a set of simulated FERENGI images of galaxies, described in the next section. These images have been classified by volunteers in Galaxy Zoo in the same way as the GZH sample. This chapter will describe how we measure a correction factor for $f_{\rm features}$ using these data as a function of redshift at fixed surface brightness, and apply the correction to the GZH sample.

4.0.2 The FERENGI sample

4.0.3 Measuring the drop in f_{features} as a function of z and μ using FERENGI data

Identifying "correctable" and "lower limit" samples.

The objective is to use the simulated data from FERENGI to predict, for a galaxy imaged at a redshift z, and with a measured $f_{\text{features},z}$ value, what its f_{features} value *would have been* if it had been viewed at $z = 0.3$. This predicted value is defined as the "debiased' vote fraction $f_{\text{features,debiased}}$, and is calculated by applying a correction to the measured value of f_{features}.

The amount that a galaxy's f_{features} vote fraction must be corrected is assumed to primarily depend on the apparent size and brightness of the galaxy. As described in 4.0.1, these factors will affect the overall clarity of the image viewed by the GZ volunteers, which in turn affects the likelihood of being able to identify distinct feature. The apparent size and brightness are controlled by both instrinsic parameters (absolute size and luminosity), and extrinsic (distance to the galaxy). The change in f_{features} then is measured as a function of redshift (z, an extrinsic freature, measuring distance to the galaxy), and surface brightness (μ, an intrinsic feature, taking into account both brightness and size).

Figure 4.1 shows the change in f_{features} for FERENGI galaxies in bins of redshift and surface brightness. Points in each z, μ represent individual FERENGI galaxies. On the x-axis of each bin is the value of f_{features} measured in that galaxy's $z = 0.3$ image (the lowest redshift of the simulated images). On the y-axis of each bin is the value of f_{features} measured in that galaxy's $z = z$ image, where z corresponds to the redshift associated with that bin. As predicted, the value of f_{features} measured at a higher redshift, z, is, in general, *lower* than the value measured at lower redshift, $z = 0.3$, *for the same galaxy.* This effect is strongest as redshift increases (to the right in Figure 4.1) and as surface brightness decreases (upwards in Figure 4.1).

A reliable predicted value can be obtained so long as the relationship between $f_{\text{features},z}$ and $f_{\text{features},z=0.3}$ is single-valued; that is, for a given $f_{\text{features},z}$, there is exactly one corresponding value of f_{features} at $z = 0.3$. Unfortunately, this is *not* always the case. Figure 4.2 shows f_{features} measured at $z = 1$ vs f_{features} measured at $z = 0.3$ for

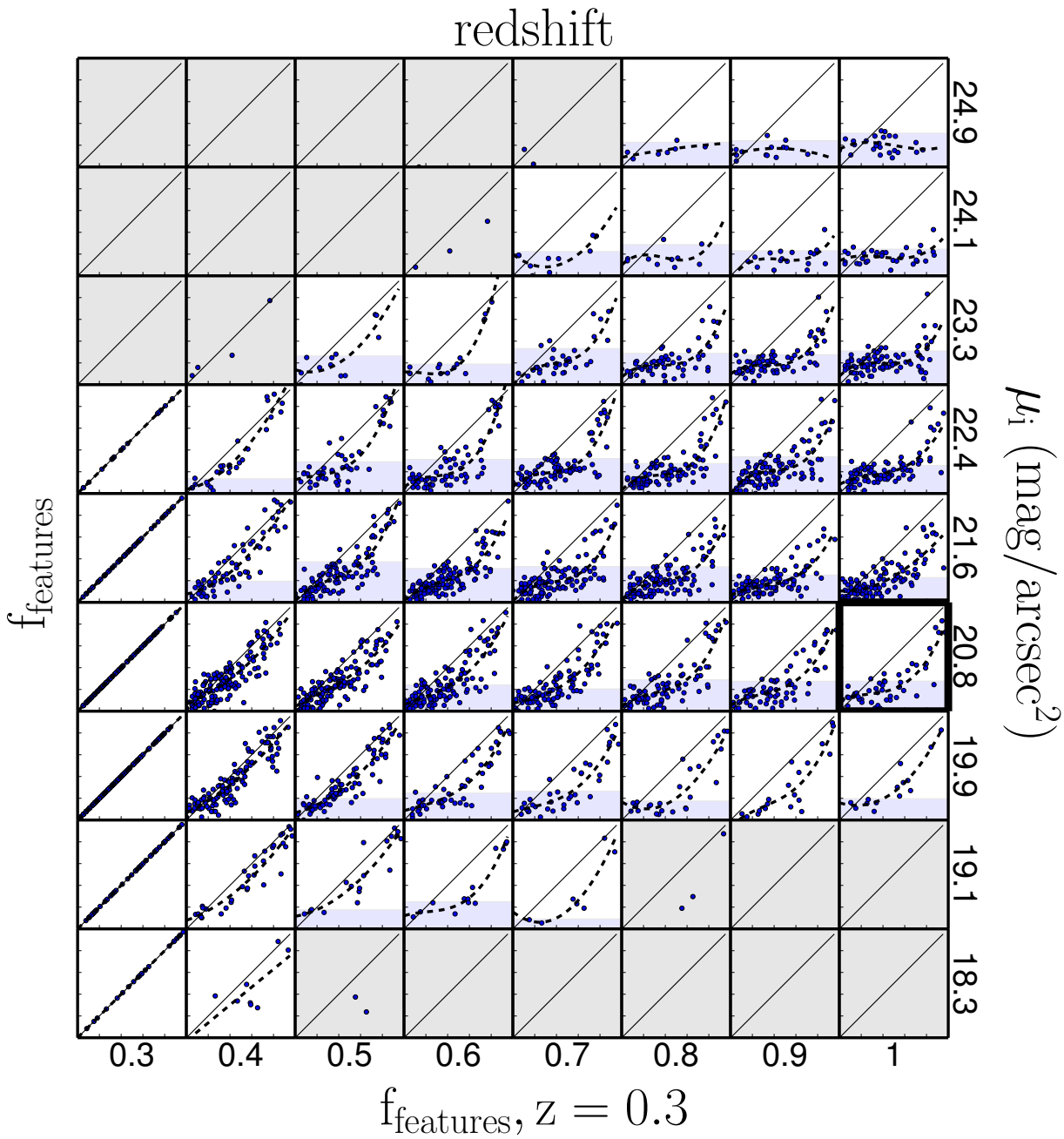

Figure 4.1 Effects of redshift bias in 3,449 images in the FERENGI sample. Each point *in a given redshift and surface brightness bin* represents a unique galaxy. On the y-axis in each bin is the $f_{\rm features}$ value of the image of that galaxy redshifted to the value corresponding to that redshift bin. On the x-axis is the $f_{\rm features}$ value of the image of the same galaxy redshifted to $z = 0.3$. The dashed black lines represent the best-fit polynomials to the data in each square. The solid black line represents $f_{{\rm features},z}$=$f_{{\rm features},z=0.3}$. Regions in which there is a single-valued relationship between $f_{\rm features}$ at high redshift and at $z = 0.3$ are white; those in which there is not are blue, and those with not enough data ($N < 5$) are grey. A larger version of the bin outlined at $z = 1.0$ and $20.3 < \mu < 21.0$ (mag/arcsec^2) is shown in Figure 4.2.

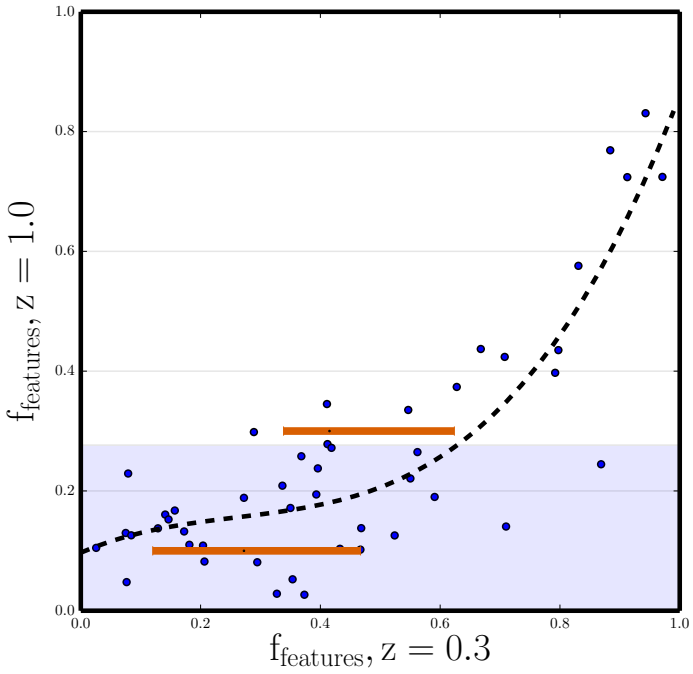

Figure 4.2 A larger version of the dark-outlined square in Figure 4.1, containing FERENGI galaxies that have been artificially redshifted to $z = 1.0$ and have surface brightnesses between $20.3 < \mu < 21.0$ (mag/arcsec^2). The orange bars represent the inner 68% (1σ) of the uncorrectable f_{features} quantiles, which are used to compute the limits on the range of debiased values.

FERENGI galaxies with average surface brightnesses $< \mu >= 20.8$ (a zoomed-in version of the dark outlined bin in Figure 4.1). This figure shows that if the value of $f_{\rm features}$ measured for a galaxy at $z = 1$ is particularly low, there is a wide range that $f_{\rm features}$ could have been if measured at $z = 0.3$. Therefore, a low measured value of $f_{\rm features}$ at high redshift could represent two morphological types of galaxies: 1) The galaxy has no distinguishable features and may be classified as a smooth elliptical, or 2) the galaxy *does* have features, but these have become blurred and too difficult to detect at high redshift.

It is important to identify such regions of surface brightness/redshift/$f_{\rm features}$ space since vote fractions cannot be confidentely corrected to a single value for galaxies in these regions. The criteria for determining whether a region of this space is single-valued, and therefore correctable, is as follows: In each surface brightness and redshift bin, the relationship between $f_{{\rm features},z}$ and $f_{{\rm features},z=0.3}$ is modelled by fitting the data with polynomials of degress n=3,2, and 1, and using the best formal fit out of the three as measured by the sum of the residuals. These fits are shown as the dashed black lines in Figures 4.1 and 4.2. Flat regions of the bins are areas in which there is *not* a clear single-valued relationship between $f_{{\rm features},z}$ and $f_{{\rm features},z=0.3}$. This is quantified by measuring the slope of the best-fit polynomial to the vote fractions; regions of the bins with a slope less than 0.4 are considered *not* one-to-one, and therefore $f_{{\rm features},z}$ cannot be boosted to its $f_{{\rm features},z=0.3}$ value. These are colored blue in Figure 4.1 and are referred to as the *lower limit* sample, because the most stringent correction available is that the weighted $f_{\rm features}$ is a lower limit to the true value.

The unshaded regions of Figure4.2 define descrete ranges of redshift, surface brightness, and $f_{\rm features}$ within which a galaxy must lie in order for the debiased vote fraction to be confidentely applied. While the appropriate correctable regions were defined as discrete bins, the true correctable region is assumed to be a smooth function of z, μ, and $f_{\rm features}$. To define this smooth space, a convex hull was calculated to enclose the correctable and lower-limit FERENGI galaxies in the $z - \mu - f_{\rm features}$ space (see Figure 4.3). The space defined by this hull was used to ultimately separate the GZH galaxies into correctable samples (those for which a correction to $f_{\rm features}$ can confidentely be applied, see next section) and lower-limit samples (those for which a single-valued correction cannot be applied). The final categorization of the GZH sample, split by imaging survey,

Table 4.1 Number of correctable galaxies for the top-level task in GZH, split by *HST* survey.

	Correction type	AEGIS	COSMOS	GEMS	GOODS-N 5-epoch	GOODS 5-epo
correctable	0	2,908	21,169	2,802	1,459	1,1
lower-limit	1	833	5,169	1,021	1,377	1,2
no correction needed ($z \leq 0.3$)	2	955	10,870	1,175	415	4
not enough information (NEI)	3	2,677	43,058	3,559	2,077	2,1
no redshift information	4	1,134	4,688	530	687	1
total		8,507	84,954	9,087	6,015	5,1

is shown in Table 4.1.

For the "lower limit" galaxies, since a single debiased f_{features} value cannot be confidentely assigned, a *range* of debiased values is estimated. In each z, μ bin in Figure 4.1, the spread of intrinsic values of $f_{\text{features},z=0.3}$ for five quantiles of observed f_{features} is computed - these are denoted by the gray lines in the close-up Figure 4.2. The range of intrinsic values of f_{features} is defined by the upper and lower 1 σ limits, enclosing the inner 68% of the data; this is represented by the orange bars in Figure 4.2. For any galaxy which cannot be directly debiased, these ranges are used to denote the upper and lower limits on the expected values $f_{\text{features},z=0.3}$ as a function of the observed f_{features}.

Computing debiased f_{features} for the "correctable" sample using the ζ equation

For the "correctable" sample of simulated FERENGI galaxies, an equation is derived to model the dropoff in f_{features} with redshift for each galaxy. Such a model is assumed to have the following criteria: (1) For a given galaxy, f_{features} should decrease relative to its $f_{\text{features},z=0.3}$ as redshift increases. (2) The corrected f_{features} value must be contained within 0 and 1, since it is a fraction. (3) The degree of dropoff may depend on the surface brightness of the galaxy. Given these three assumptions, a simple exponential function was derived:

$$f_{\mu,z} = 1 - (1 - f_{\mu,z=0.3})e^{\frac{z-z_0}{\zeta}} \tag{4.1}$$

where $f_{\mu,z=0.3}$ is the vote fraction at the lowest redshift in the artificially-redshifted

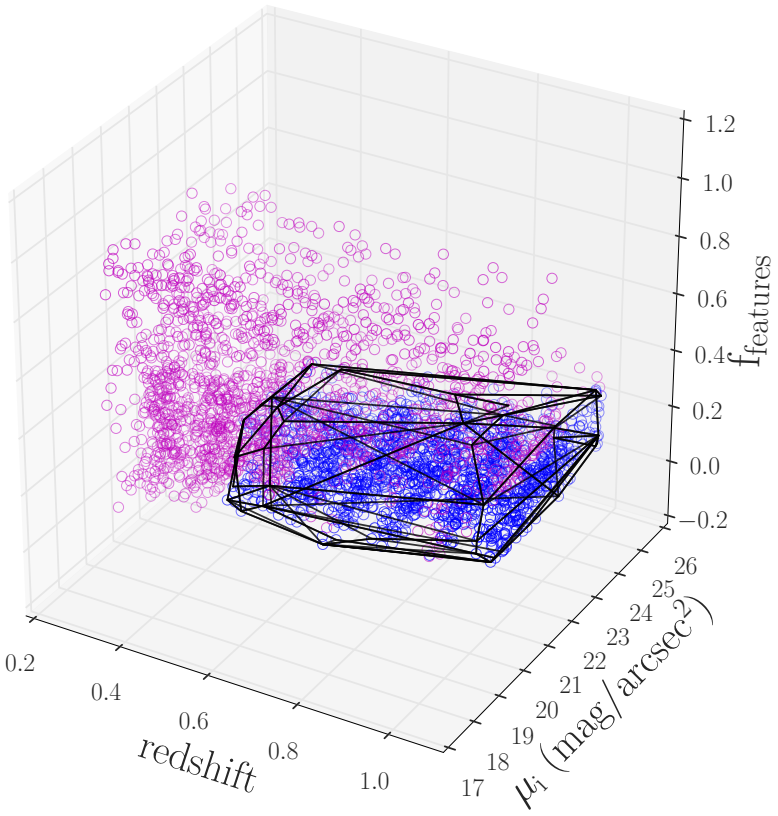

Figure 4.3 The final separation of the correctable and lower-limit samples in redshift/surface brightness/$f_{\rm features}$ space.**Pink** points are all FERENGI galaxies in the **unshaded** regions of Figure 4.1. **Blue** points are all FERENGI galaxies in the **blue shaded** regions of Figure 4.1. The solid black line is the convex hull which encloses the uncorrectable points and defines the region of the lower-limit sample.

FERENGI sample ($z_0 = 0.3$). ζ is a parameter that controls the rate at which f_{features}decreases with redshift.

Equation 4.1 is then fit to each galaxy in the "correctable" FERENGI sample, and ζ is measured for each. Figure 4.4 shows the best fit equations for 16 galaxies, and the ζ corresponding to the best fit is displayed with each galaxy. As it was assumed that surface brightness likely plays a role in the level of dropoff in f_{features}, and hence the value of ζ which controls this dropoff, it is assumed that ζ follows a simple linear dependence with surface brightness:

$$\log_{10}(\hat{\zeta}) = \zeta_0 + (\zeta_1 \times \mu), \tag{4.2}$$

where $\hat{\zeta}$ is the correction factor applied to each galaxy. Figure 4.5 shows the relationship between the derived ζ values and the surface brightness μ of the FERENGI galaxies, which is fit with equation 4.2. The best-fit parameters to this linear fit from least-squares optimization are $\zeta_0 = 0.50$, $\zeta_1 = -0.03$. Interestingly, only a very weak surface brightness dependence is detected. It is difficult to determine from these data whether the weak detection is due to a true lack of dependence, or insufficient data (only 28 galaxies had sufficient data to accurately measure ζ).

Using the ζ parameters measured in the FERENGI sample, a final debiased correction equation is derived to correct the f_{features} vote fractions in the HST data:

$$f_{\text{features,debiased}} = 1 - (1 - f_{\text{features,weighted}})e^{\frac{-(z-z_0)}{\hat{\zeta}}} \tag{4.3}$$

where $f_{\text{features,weighted}}$ is the weighted vote fraction, and $f_{\text{features,debiased}}$ is bounded between $f_{\text{features,weighted}}$ and 1.

Results and the NEI sample: limitations of the ferengi simulated data

- show table of HST sample breakdown 4.1
- show how above method only works for HST galaxies with z/mu corresponding to ferengi space 4.7
- discuss why ferengi can't completely replicate mu distribution of HST (cite Karen response to referee)

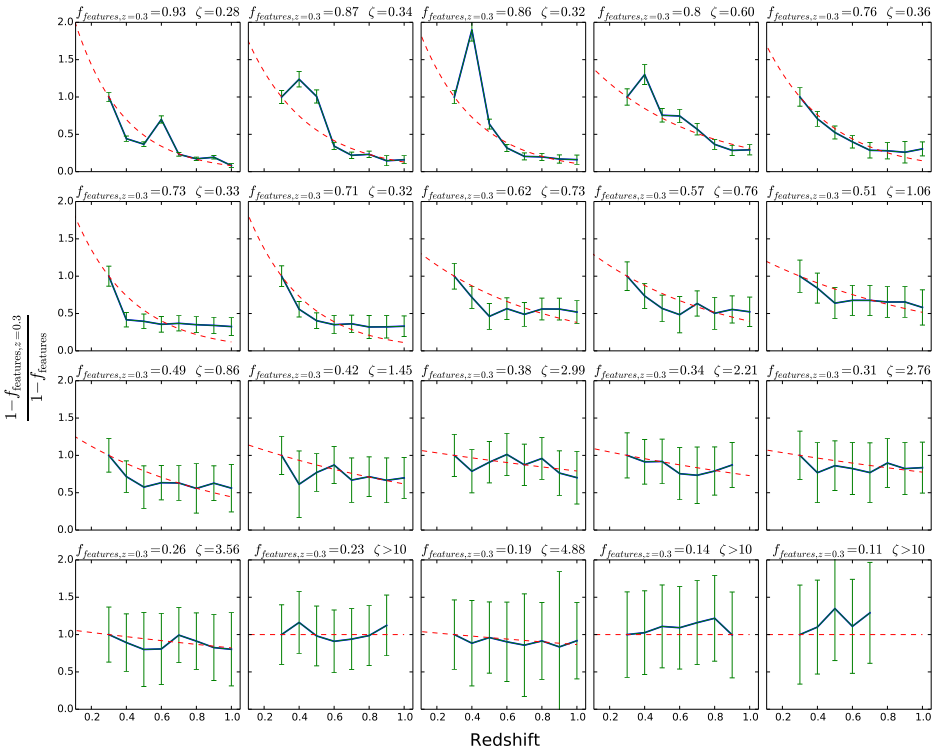

Figure 4.4 Behaviour of the normalised, weighted vote fractions of features visible in a galaxy (f_{features}) as a function of redshift in the artificial FERENGI images. Galaxies in this plot were randomly selected from a distribution with evolutionary correction $e = 0$ and at least three detectable images in redshift bins of $z \geq 0.3$. The displayed bins are sorted by $f_{\mathrm{features},z=0.3}$, labeled above each plot. Measured vote fractions (blue solid line) are fit with an exponential function (red dashed line; Equation 4.1); the best-fit parameter for ζ is given above each plot.

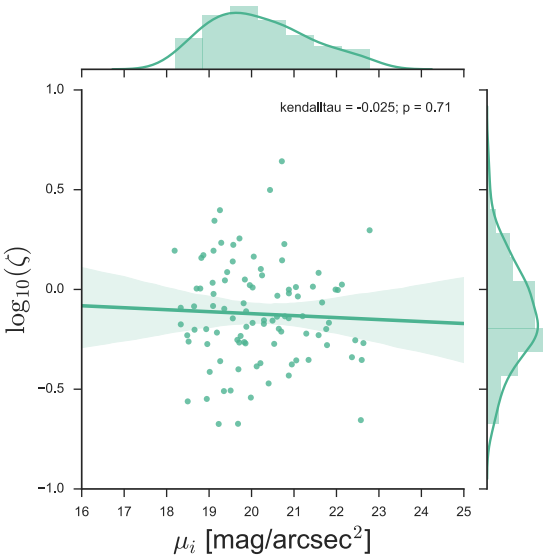

Figure 4.5 All fits for the FERENGI galaxies of the vote fraction dropoff parameter ζ for f_{features} as a function of surface brightness. This includes only the simulated galaxies with a bounded range on the dropoff ($-10 < \zeta < 10$) and sufficient points to fit each function (28 original galaxies, each with varying images artificially redshifted in one to eight bins over a range from $0.3 \lesssim z_{\text{sim}} \lesssim 1.0$).

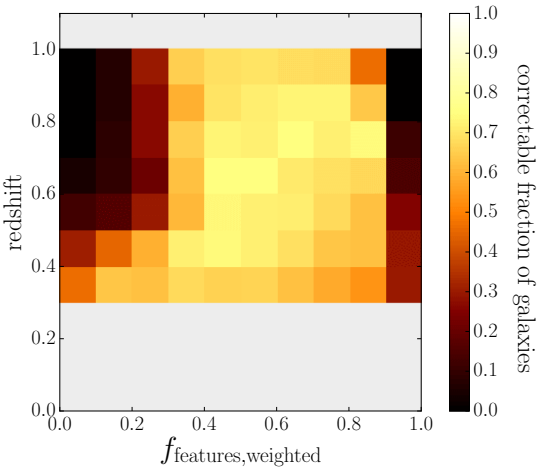

Figure 4.6 Histogram showing the fraction of galaxies that have a finite correction for the debiased vote fractions $f_{\text{features,debiased}}$ as a function of f_{features} and redshift. The parameter space for corrections is limited to $0.3 \leq z \leq 1.0$ due to the sampling of the parent SDSS galaxies and detectability in the FERENGI images.

- discuss limits shown in 4.6

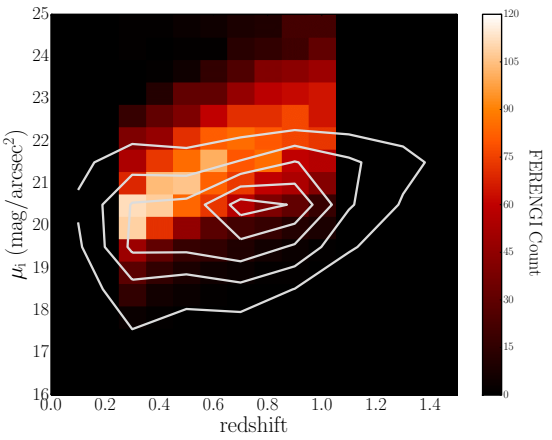

Figure 4.7 Surface brightness as a function of redshift for 3,449 FERENGI images and the 102,548 `main` galaxies with measured μ and z values. The colour histogram shows the number of FERENGI images as a function of μ and $z_{\rm sim}$. White contours show counts for the galaxies in the `main` sample, with the outermost contour starting at $N = 1500$ and separated by intervals of 1500.

Chapter 5

GZH red disk fraction

red disk fraction project

Chapter 6

Summary & Future Work

References

Muzahid, S., Kacprzak, G. G., Churchil, C. W., et al. 2015, 15